Highly anisotropic thermal conductivity of arsenene: An *ab initio* study

Majid Zeraati,[1] S. Mehdi Vaez Allaei,[1,2,*] I. Abdolhosseini Sarsari,[3] Mahdi Pourfath,[4,5] and Davide Donadio[6,7,8,9,†]

[1]*Department of Physics, University of Tehran, Tehran 14395-547, Iran*

[2]*School of Physics, Institute for Research in Fundamental Sciences, Tehran 19395-5531, Iran*

[3]*Department of Physics, Isfahan University of Technology, Isfahan 84156-83111, Iran*

[4]*School of Electrical and Computer Engineering, University of Tehran, Tehran 14395-515, Iran*

[5]*Institute for Microelectronics, TU Wien, Gußhausstraße 27–29/E360, 1040 Vienna, Austria*

[6]*Department of Chemistry, University of California, Davis, One Shields Avenue, Davis, California 95616, USA*

[7]*Max-Planck-Institut für Polymerforschung, Ackermannweg 10, D-55128 Mainz, Germany*

[8]*Donostia International Physics Center, Paseo Manuel de Lardizabal, 4, 20018 Donostia-San Sebastian, Spain*

[9]*IKERBASQUE, Basque Foundation for Science, E-48011 Bilbao, Spain*

(Received 20 July 2015; revised manuscript received 29 December 2015; published 16 February 2016)

Elemental two-dimensional (2D) materials exhibit intriguing heat transport and phononic properties. Here we have investigated the lattice thermal conductivity of newly proposed arsenene, the 2D honeycomb structure of arsenic, using *ab initio* calculations. Solving the Boltzmann transport equation for phonons, we predict a highly anisotropic thermal conductivity of 30.4 and 7.8 W/mK along the zigzag and armchair directions, respectively, at room temperature. Our calculations reveal that phonons with mean free paths between 20 nm and 1 μm provide the main contribution to the large thermal conductivity in the zigzag direction; mean free paths of phonons contributing to heat transport in the armchair directions range between 20 and 100 nm. The obtained anisotropic thermal conductivity and feasibility of synthesis, in addition to high electron mobility reported elsewhere, make arsenene a promising material for nanoelectronic applications and thermal management.

DOI: 10.1103/PhysRevB.93.085424

I. INTRODUCTION

The discovery of graphene as a stable atomically thin material has led to extensive investigation of similar two-dimensional (2D) systems. Its properties such as high electron mobility [1] and very high thermal conductivity [2–5] make graphene very appealing for applications in electronics for packaging and thermal management [6–11]. The successful isolation of single-layer graphene fostered the search for further ultrathin 2D structures, such as silicene, germanene, phosphorene, and transition-metal dichalcogenides, e.g., MoS_2 and WS_2 [12,13]. These materials are now considered for various practical usages due to their distinguished properties stemming from their low dimensionality. Thermal transport in 2D materials has recently attracted the attention of the scientific community, as anomalous heat conduction has been predicted to occur in systems with reduced dimensionality [14]. Phononic properties and thermal conductivity vary significantly from one 2D system to another [5,15–18]. For example, silicene has a buckled structure and a much lower thermal conductivity [16,19] compared to graphene [12,20,21].

Two-dimensional structures of arsenic and phosphorous have recently been investigated [22–26]. Arsenic and phosphorus are in the fifth group of the periodic table, and both have different allotropes. Black phosphorus is a layered allotrope of phosphorus similar to graphite, and the stability of its single-layer form, named *phosphorene*, has been probed both theoretically and experimentally [13,27]. *Gray arsenic* is one of the most stable allotropes of arsenic with a buckled layered structure [26,28]. In addition, arsenic has an orthorhombic phase (puckered) similar to black phosphorus [22,24,25], and its monolayer is called *arsenene* (see Fig. 1). Experimental observations have shown that gray arsenic undergoes a structural phase transition to the orthorhombic precursor of arsenene at temperatures of about $T = 370$ K [29]. As a monolayer, arsenene can have a direct band gap of the order of 1 eV, as opposed to the multilayer allotrope, which exhibits an indirect band gap [22,25]. According to our calculations, arsenene is stable as a puckered monolayer also near zero temperature, in agreement with previous reports [22,24,25]. Both phosphorene and arsenene exhibit diverse polymorphs, with electronic properties that vary from semiconducting to semimetallic and metallic as a function of structure and strain [22,26,30]. Low dimensionality and the versatility of their electronic structure make two-dimensional fifth-group elemental systems very appealing not only for fundamental studies but also for practical applications in nanoelectronics. For the latter applications, it is, however, essential to characterize thermal transport and heat dissipation to predict their operating temperatures.

In this paper we investigate heat conduction in arsenene, and we elucidate the anisotropy of its thermal conductivity. We consider "puckered" unstrained arsenene, which is a semiconductor [22]. Since in semiconductors phonons are the predominant heat carriers, we use first-principles anharmonic lattice dynamics calculations and the Boltzmann transport equation to compute phonon dispersion relations and thermal conductivity. According to electronic structure calculations [22], arsenene has a band gap of the order of 1 eV; thus we expect a negligible electronic contribution to κ, unless the system is doped or strained. For this reason we restrict our study to the phononic contribution to thermal transport.

*smvaez@ut.ac.ir

†ddonadio@ucdavis.edu

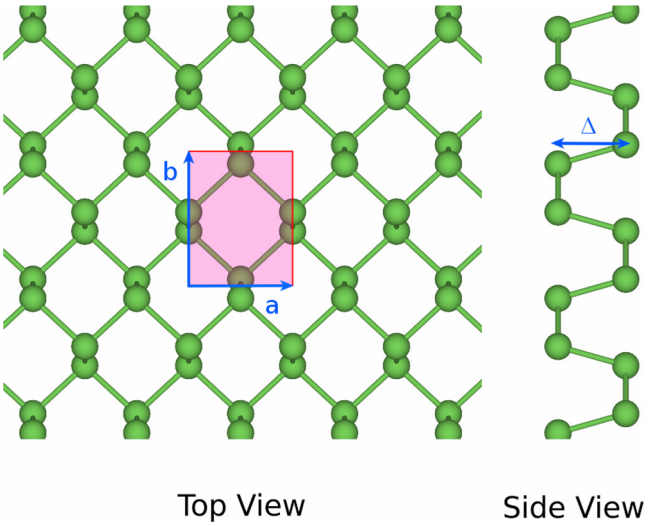

FIG. 1. Top and side views of puckered arsenene.

II. RESULTS AND DISCUSSION

A. Structural properties

We employ density functional theory (DFT) as implemented in the VASP code [31] with projector-augmented-wave (PAW) [32] pseudopotentials and the Perdew-Burke-Ernzerhof (PBE) generalized gradient functional [33] exchange-correlation functional. Integration over the Brillouin zone is performed using a 15×15×1 Γ-center Monkhorst-Pack mesh of k points [34], and plane waves up to an energy cutoff of 360 eV are used as a basis set to represent the Kohn-Sham wave functions. The simulation cell is built with a vacuum layer of 10 Å, which is sufficient to avoid interactions between periodic images. Detailed convergence studies with respect to the above-mentioned parameters are provided in the Supplemental Material [35]. The structural relaxations were performed by using the conjugate-gradient (CG) algorithm with a convergence criterion of 10^{-6} eV/Å for the maximum residual force component per atom.

As shown in Fig. 1, arsenene has a puckered structure arranged in a rectangular unit cell with *Pmna* symmetry and lattice vectors $a = 3.686$ Å and $b = 4.769$ Å. The in-plane bond length between atoms (c_1) is 2.510 Å, while the bonding length between atoms in different planes (c_2) is 2.496 Å. The distance between the two planes is denoted by Δ and is 2.402 Å. Our structural parameters are compared with previous studies in Table I. We observe very small discrepancies with previous calculations, less than 0.05 Å, even when different functionals are used, indicating that the structure is not very sensitive to the flavor of DFT adopted.

B. Harmonic lattice dynamics

We have utilized the PHONOPY package [36] interfaced with VASP to compute inter-atomic force constants (IFCs). After testing convergence of the phonon frequencies as a function of the size of the supercell [37], an 8×8×1 supercell has been adopted, with a 3×3×1 Γ-center Monkhorst-Pack mesh of k points, to build the dynamical matrix $\mathcal{D}$ (see Supplemental Material for details). Second derivatives of the potential energy

TABLE I. The lattice parameters of arsenene: a and b are the lattice vectors, Δ is the puckering distance, c_1 is the bond length between atoms that are in the same plane, and c_2 is the bond length between atoms that are in different planes.

Monolayer of arsenene					
Method	a (Å)	b (Å)	Δ (Å)	c_1 (Å)	c_2 (Å)
PBE	3.686	4.769	2.402	2.510	2.496
PBE (Ref. [22])	3.677	4.765	2.441	2.521	2.485
revPBE-vdW (Ref. [25])	3.68	4.80		2.51	2.49

are computed by finite differences displacing the atoms by 10^{-3} Å. $\mathcal{D}$ is symmetrized, and translational invariance is ensured by imposing the acoustic sum rule. The frequencies of the vibrational modes are obtained by diagonalizing $\mathcal{D}$, and the phonon dispersion curves are represented in Fig. 2. The absence of phonon branches with imaginary frequencies indicates the stability of the system at zero temperature.

The phonon bands exhibit two acoustic modes, a longitudinal one (LA) and an in-plane transverse one (TA), with linear dispersion ($\omega \propto q$) for $q \to 0$, and an out-of-plane flexure mode (ZA) with quadratic dispersion in the long-wavelength limit, which is a general feature of 2D membranes [38]. Flexural modes have been characterized in graphene [15,39], silicene [16,40], hexagonal boron nitride (h-BN) [41], MoS_2 [42], and ultrathin silicon membranes [43,44]. Flexural modes have a major role in contributing to the thermal conductivity of graphene, both as carriers [15] and as scatterers [45]. In addition, we observe a gap of about 2 THz between the low-frequency and high-frequency optical branches, which has an impact on the selection rules that determine the coupling terms of three-phonon scattering processes.

C. Thermal conductivity

We have computed the thermal conductivity of arsenene by solving the phonon Boltzmann transport equation (BTE) with an iterative self-consistent algorithm [46,47], using the ShengBTE package [48]. In our calculations we have considered

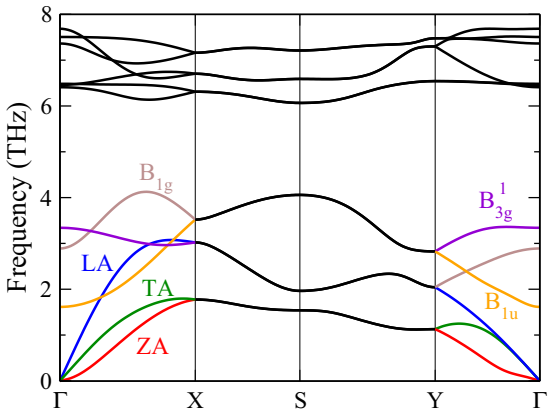

FIG. 2. Phonon dispersion curves along the high-symmetry directions of the first Brillouin zone for puckered arsenene.

third-order interatomic force constants up to the fourth shell of neighbors in a 5×5×1 supercell [49] with a 3×3×1 Γ-centered Monkhorst-Pack mesh of k points, which corresponds to the 15×15×1 mesh used for the structural calculations in the unit cell. Convergence tests are reported in the Supplemental Material.

Third derivatives of the potential energy with respect to displacements of atoms ijk along $\alpha\beta\gamma$ coordinates are also computed by finite differences, and translational invariance is enforced by imposing $\sum_i \Phi_{ijk}^{\alpha\beta\gamma} = 0$, following the procedure described by Li *et al.* [50].

Three phonon scattering processes have been considered in the calculation of phonon lifetimes τ_λ^0 in the relaxation-time approximation (RTA) according to the following expression [48,51]:

$$\frac{1}{\tau_\lambda^0} = \frac{1}{N}\left(\sum_{\lambda'\lambda''}^{+}\Gamma^{+}_{\lambda\lambda'\lambda''} + \frac{1}{2}\sum_{\lambda'\lambda''}^{-}\Gamma^{-}_{\lambda\lambda'\lambda''} + \sum_{\lambda'}\Gamma^{\mathrm{ext}}_{\lambda\lambda'}\right), \quad (1)$$

where $\Gamma^{+}_{\lambda\lambda'\lambda''}$ and $\Gamma^{-}_{\lambda\lambda'\lambda''}$ represent the scattering rates due to absorbing and emitting three-phonon intrinsic processes, respectively. The extrinsic scattering term $\Gamma^{\mathrm{ext}}_{\lambda\lambda'}$ does not include isotope scattering since arsenic does not present isotopic disorder, and defects were not considered. $\Gamma^{\mathrm{ext}}_{\lambda\lambda'}$ is, however, used to take into account boundary scattering processes later on.

To properly take into account collective effects in phonon transport in two-dimensional materials, it is necessary to solve the linearized BTE exactly, which is here performed self-consistently. Self-consistent phonon lifetimes are therefore expressed as [50–52]

$$\tau_\lambda^\beta = \tau_\lambda^0\left(1 + \Delta_\lambda^\beta\right), \quad (2)$$

with

$$\Delta_\lambda^\beta = \frac{1}{N}\left[\sum_{\lambda'\lambda''}^{+}\Gamma^{+}_{\lambda\lambda'\lambda''}\left(\chi^\beta_{\lambda\lambda''}\tau^\beta_{\lambda''} - \chi^\beta_{\lambda\lambda'}\tau^\beta_{\lambda'}\right) + \sum_{\lambda'\lambda''}^{-}\frac{1}{2}\Gamma^{-}_{\lambda\lambda'\lambda''}\left(\chi^\beta_{\lambda\lambda''}\tau^\beta_{\lambda''} + \chi^\beta_{\lambda\lambda'}\tau^\beta_{\lambda'}\right)\right], \quad (3)$$

in which $\chi^\beta_{\lambda\lambda'} = \omega_{\lambda'}v^\beta_{\lambda'}/\omega_\lambda v^\beta_\lambda$. Here we point out that τ_λ^β is the relaxation time for phonons with polarization λ that propagate in the direction β. In fact, solving BTE beyond RTA entails a directional dependence of phonon relaxation times, as the direction of the heat flux determines different shifts in the phonon population and therefore different scattering efficiencies [52]. Knowing the distribution function, the phononic thermal conductivity tensor κ is then expressed as

$$\kappa_{\alpha\beta} = \frac{1}{V}\sum_\lambda \hbar\omega_\lambda \frac{\partial f}{\partial T} v^\alpha_\lambda v^\beta_\lambda \tau^\beta_\lambda, \quad (4)$$

where f is the phonon distribution function, ω_λ is the phonon angular frequency, and v^α_λ is the velocity component along the α direction. Both the RTA and the self-consistent solutions to BTE have been obtained by integrating the Brillouin zone over a dense 100×100×1 grid of q points, which ensured convergence of the iterative procedure in the whole temperature range considered.

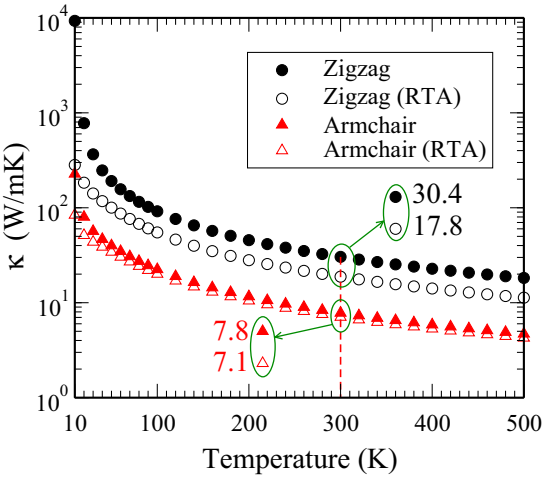

FIG. 3. Thermal conductivity of arsenene as a function of temperature along the zigzag and armchair directions. Open symbols indicate the thermal conductivity calculated using the relaxation-time approximation, while solid ones refer to self-consistent calculations.

The two diagonal components of the thermal conductivity at temperatures between 10 and 500 K are reported in Fig. 3. This plot also shows a large difference between the self-consistent and the RTA results, especially for heat transport in the zigzag direction over the whole range of temperatures considered. In the armchair direction differences are limited to temperatures below 50 K. The reason for such large differences between self-consistent and RTA results may possibly lie in the occurrence of collective phonon excitations that give rise to hydrodynamic effects [53]. Such effects have been observed not only in 2D materials with very high thermal conductivity, such as graphene, but also in MoS_2 and fluorinated graphene [5]. The thermal conductivity along the zigzag and armchair directions at $T = 300$ K is 30.4 and 7.8 W m^{-1} K^{-1}, respectively. The nearly fourfold ratio between the two components indicates a high anisotropy. The anisotropy ratio is much larger at low temperatures, $\kappa_{\mathrm{zigzag}}/\kappa_{\mathrm{armchair}} \sim 40$ at 10 K: it monotonically decreases and becomes nearly constant above 150 K.

The thermal conductivity of arsenene in comparison to graphene and hexagonal boron nitride is very low: for example, both experimental and theoretical studies indicate that the intrinsic thermal conductivity of graphene is larger than 3000 W/mK [2,3]. Due to the larger atomic weight of As, κ of arsenene is lower than that of the equivalent puckered phase of phosphorene, which is also strongly anisotropic, theoretically predicted as 110 and 36 W m^{-1} K^{-1} in the zigzag

TABLE II. Speed of sound (group velocity; in km/s) of acoustic modes of arsenene and phosphorene close to the zone center (Γ point). Since ZA modes have quadratic dispersion at the Γ point, their group velocity is zero.

	Arsenene		Phosphorene
	TA	LA	LA [18]
Armchair	2.41	2.44	4.17
Zigzag	2.41	4.77	7.73

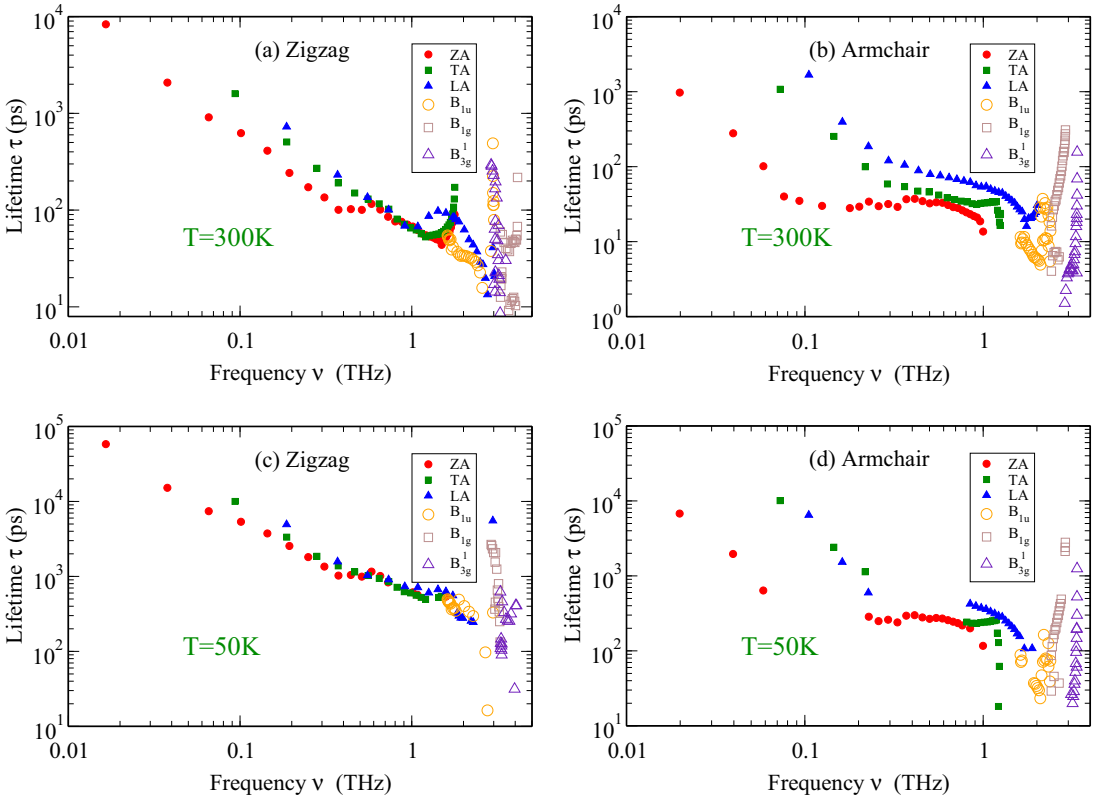

FIG. 4. Relaxation time of phonon modes as a function of frequency along the (a) zigzag and (b) armchair directions at room temperature and (c) and (d) at $T = 50$ K.

and armchair directions, respectively [18]. We note indeed that the group velocity of the acoustic modes of arsenene along both zigzag and armchair directions near the zone center are about two times smaller than those of phosphorene (see Table II). According to Eq. (4), group velocities contribute to κ quadratically, and we can argue that the difference in v_λ is mostly responsible for the difference between the thermal conductivities of arsenene and phosphorene at room temperature. In fact $v^2_{\text{phosphorene}}/v^2_{\text{arsenene}}$ is 2.7 and 2.9 for LA modes in the zigzag and armchair directions, while the thermal conductivity ratio is 3.6 and 4.6, thus indicating that significant differences occur also in phonon lifetimes, possibly originating from the different occupations of the optical modes at room temperature due to quantum effects.

Table II would also suggest that the main origin of the large anisotropy of κ lies in the difference between the group velocities of the LA mode in the zigzag and armchair directions. However, the center-zone speed of sound provides only limited insight into heat-transport mechanisms, and a more detailed analysis is required. To this scope we analyze phonon lifetimes (Fig. 4) at low temperature (50 K) and at room temperature, and we compute the contribution of each phonon branch to the total thermal conductivity as a function of temperature (Fig. 5). At both temperatures examined, along the zigzag direction, phonon lifetimes for ZA, TA, and LA modes scale as $1/\omega^a$ for $\omega \to 0$, with a between 1.4 and 1.6. Such scaling, combined with the density of state and the group velocities computed by harmonic lattice dynamics, prevents divergence of κ [45]: divergence would occur for $a \geqslant 2$. We notice that at low temperature ZA, LA, and TA propagating in the zigzag direction have lifetimes of the same order of magnitude, while at room temperature ZAs have significantly lower lifetimes. For phonons propagating along the armchair direction we observe that ZA lifetimes decay fast and eventually plateau for frequency larger than 0.1 THz. At both low and room temperatures $\tau_{ZA} \ll \tau_{LA/TA}$. Furthermore, the relaxation times of the LA modes at low frequencies, which play a significant role in the process of heat conduction at room temperature, are larger than those of other acoustic modes (see Fig. 4). The group velocity of the LA mode near the zone center

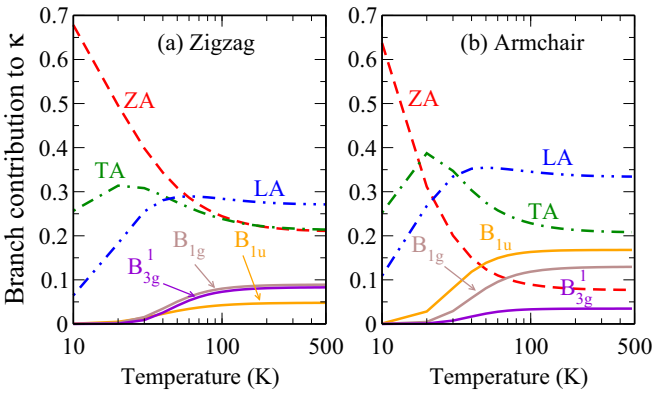

FIG. 5. Normalized contribution of each phonon branch to the total thermal conductivity as a function of temperature along the (a) zigzag and (b) armchair directions.

is the largest along the zigzag direction, while it is comparable to the TA mode along the armchair direction (see Table II). The combination of these two facts leads to the large anisotropy observed a room temperature.

From the calculation of the branch-resolved partial contribution to κ, reported in Fig. 5, we observe that the ZA mode provides the largest contribution along both directions at low temperatures, in spite of relatively small lifetimes: this is due to the large density of state of ZA modes at low frequency, which are the ones populated at low temperature. This contribution rapidly decreases as the temperature increases and reaches ∼8% (armchair direction) and ∼20% (zigzag) for temperatures above 300 K. This is in contrast to the case of graphene, where the ZA modes provide the main contribution to heat conduction even at high temperatures [15]. Due to the selection rules of phonon scattering in graphene, originating from the combination of low dimensionality and hexagonal symmetry, ZA modes have a very large relaxation time compared to the in-plane acoustic branches [15]. In contrast, due to its puckered structure, similar to silicene and phosphorene [16,18], the hexagonal symmetry is broken in arsenene, resulting in larger scattering rates and shorter relaxation times of the ZA modes. The contribution of the ZA modes remains, however, substantial and roughly equivalent to that of the TA modes in the zigzag direction, while it drops below 10% in the armchair direction. At temperatures higher than 100 K, the contribution of LA modes to the thermal conductivity is the largest in both directions. These results suggest that the origin of the anisotropy of κ is different depending on temperature: at high-temperature anisotropy it is mostly determined by the different group velocities of the LA modes, which provide the main contribution to κ, whereas at low temperature it stems from the difference between the relaxation times of the ZA modes. Such differences account for the much larger anisotropy ratios at low temperature evidenced by the calculation of κ.

Finally, we computed the thermal conductivity accumulation function $\kappa(\lambda)$ as a function of phonon mean free paths as the sum of the contributions to κ from phonons with mean free path smaller than λ, as obtained from the self-consistent solution of the BTE. These calculations can be compared to thermal conductivity spectroscopy measurements [54,55] and provide an estimate of the range of phonon mean free paths that mostly contribute to κ. The results reported in Fig. 6 indicate a broadband contribution to κ in both the armchair and zigzag directions. In contrast to other 2D materials with high κ, such as graphene, graphane, and h-BN, which exhibit a significant contribution to κ from phonons with mean free paths larger than several microns [5], for arsenene 90% of the thermal conductivity contribution comes from mean free paths smaller than 550 and 440 nm for conduction in the zigzag and armchair directions. The center of the distribution of the mean free paths contributing to κ is ∼90 and ∼50 nm in the zigzag and armchair directions. We therefore expect a significant reduction of κ in polycrystalline arsenene sheets in both directions for grain size of the order of 100 nm or less. In addition, the presence of point or line defects that would scatter phonons with mean free paths between 50 and 100 nm would have a more prominent effect on transport in the zigzag direction, thus suppressing anisotropy.

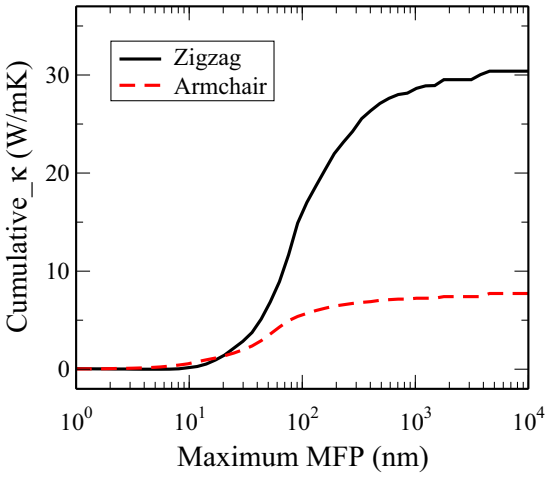

FIG. 6. Cumulative thermal conductivity as a function of phonon mean free path at $T = 300$ K along the zigzag and armchair directions.

III. CONCLUSIONS

In summary we have theoretically investigated the phonon properties and the thermal conductivity of arsenene by *ab initio* anharmonic lattice dynamics. According to our calculations arsenene is one of the elemental 2D materials with the lowest thermal conductivity, especially if we consider the armchair component. The larger mass of arsenic atoms compared to phosphorus leads to a 3 times smaller thermal conductivity of this material compared to phosphorene. Compared to phosphorene, the thermal conductivity of arsenene is even more strongly anisotropic. Such anisotropy could be exploited for heat management in nanoelectronic devices if one wants to establish directional heat dissipation. Unlike graphene, the longitudinal acoustic phonon modes provide the main contribution to the thermal conductivity of arsenene at temperatures above 100 K, which is mainly due to the puckered structure of this material. From this observation, we expect that κ of arsenene would be less affected by the interaction with a substrate than in those materials for which the main contribution comes from flexural modes.

ACKNOWLEDGMENT

The work of S.M.V.A. was supported in part by the Research Council of the University of Tehran.

[1] K. S. Novoselov, A. K. Geim, S. V. Morozov, D. Jiang, M. I. Katsnelson, I. V. Grigorieva, S. V. Dubonos, and A. A. Firsov, Nature (London) **438**, 197 (2005).

[2] X. Xu, L. F. C. Pereira, Y. Wang, J. Wu, K. Zhang, X. Zhao, S. Bae, C. Tinh Bui, R. Xie, J. T. L. Thong, B. H. Hong, K. P. Loh, D. Donadio, B. Li, and B. Özyilmaz, Nat. Commun. **5**, 3689 (2014).

[3] G. Fugallo, A. Cepellotti, L. Paulatto, M. Lazzeri, N. Marzari, and F. Mauri, Nano Lett. **14**, 6109 (2014).

[4] L. Lindsay, W. Li, J. Carrete, N. Mingo, D. A. Broido, and T. L. Reinecke, Phys. Rev. B **89**, 155426 (2014).

[5] A. Cepellotti, G. Fugallo, L. Paulatto, M. Lazzeri, F. Mauri, and N. Marzari, Nat. Commun. **6**, 6400 (2015).

[6] P. Wei, W. Bao, Y. Pu, C. N. Lau, and J. Shi, Phys. Rev. Lett. **102**, 166808 (2009).

[7] Y. M. Zuev, W. Chang, and P. Kim, Phys. Rev. Lett. **102**, 096807 (2009).

[8] C.-R. Wang, W.-S. Lu, L. Hao, W.-L. Lee, T.-K. Lee, F. Lin, I.-C. Cheng, and J.-Z. Chen, Phys. Rev. Lett. **107**, 186602 (2011).

[9] A. Rajabpour, S. M. Vaez Allaei, and F. Kowsary, Appl. Phys. Lett. **99**, 051917 (2011).

[10] A. Rajabpour and S. M. Vaez Allaei, Appl. Phys. Lett. **101**, 053115 (2012).

[11] Z. Yan, G. Liu, J. M. Khan, and A. A. Balandin, Nat. Commun. **3**, 827 (2012).

[12] A. K. Geim and I. V. Grigorieva, Nature (London) **499**, 419 (2013).

[13] J. Guan, Z. Zhu, and D. Tománek, Phys. Rev. Lett. **113**, 046804 (2014).

[14] S. Lepri, R. Livi, and A. Politi, Phys. Rep. **377**, 1 (2003).

[15] L. Lindsay, D. A. Broido, and N. Mingo, Phys. Rev. B **82**, 115427 (2010).

[16] H. Xie, M. Hu, and H. Bao, Appl. Phys. Lett. **104**, 131906 (2014).

[17] W. Li, J. Carrete, and N. Mingo, Appl. Phys. Lett. **103**, 253103 (2013).

[18] A. Jain and A. J. H. McGaughey, Sci. Rep. **5**, 8501 (2015).

[19] K. Yang, S. Cahangirov, A. Cantarero, A. Rubio, and R. D'Agosta, Phys. Rev. B **89**, 125403 (2014).

[20] L. Chen, C.-C. Liu, B. Feng, X. He, P. Cheng, Z. Ding, S. Meng, Y. Yao, and K. Wu, Phys. Rev. Lett. **109**, 056804 (2012).

[21] P. Vogt, P. De Padova, C. Quaresima, J. Avila, E. Frantzeskakis, M. C. Asensio, A. Resta, B. Ealet, and G. Le Lay, Phys. Rev. Lett. **108**, 155501 (2012).

[22] C. Kamal and M. Ezawa, Phys. Rev. B **91**, 085423 (2015).

[23] S. Zhang, Z. Yan, Y. Li, Z. Chen, and H. Zeng, Angew. Chem. **127**, 3155 (2015).

[24] Z. Y. Zhang, H. N. Cao, J. C. Zhang, Y. H. Wang, D. S. Xue, and M. S. Si, AIP Adv. **5**, 067117 (2015).

[25] Z. Zhang, J. Xie, D. Yang, Y. Wang, M. Si, and D. Xue, Appl. Phys. Express **8**, 055201 (2015).

[26] Z. Zhu, J. Guan, and D. Tománek, Phys. Rev. B **91**, 161404 (2015).

[27] H. Liu, A. T. Neal, Z. Zhu, Z. Luo, X. Xu, D. Tománek, and P. D. Ye, ACS Nano **8**, 4033 (2014).

[28] O. Madelung, *Semiconductors: Data Handbook* (Springer, Berlin, 2004).

[29] H. Thurn and H. Krebs, Acta Crystallogr. Sect. B Struct. Crystallogr. Cryst. Chem. **25**, 125 (1969).

[30] A. S. Rodin, A. Carvalho, and A. H. Castro Neto, Phys. Rev. Lett. **112**, 176801 (2014).

[31] G. Kresse and J. Furthmüller, Phys. Rev. B **54**, 11169 (1996).

[32] P. E. Blöchl, Phys. Rev. B **50**, 17953 (1994).

[33] J. P. Perdew, K. Burke, and M. Ernzerhof, Phys. Rev. Lett. **77**, 3865 (1996).

[34] H. J. Monkhorst and J. D. Pack, Phys. Rev. B **13**, 5188 (1976).

[35] See Supplemental Material at http://link.aps.org/supplemental/10.1103/PhysRevB.93.085424 for details on the convergence for different quantities (vacuum size, k-points, κ and cubic force constants).

[36] A. Togo, F. Oba, and I. Tanaka, Phys. Rev. B **78**, 134106 (2008).

[37] We have verified that a $6\times6\times1$ supercell is already sufficient to get converged phonon dispersion relations without imaginary frequencies.

[38] H. Zabel, J. Phys.: Condens. Matter **13**, 7679 (2001).

[39] J.-W. Jiang, B.-S. Wang, J.-S. Wang, and H. S. Park, J. Phys.: Condens. Matter **27**, 083001 (2015).

[40] S. Cahangirov, M. Topsakal, E. Aktürk, H. Sahin, and S. Ciraci, Phys. Rev. Lett. **102**, 236804 (2009).

[41] L. Lindsay and D. A. Broido, Phys. Rev. B **84**, 155421 (2011).

[42] Y. Cai, J. Lan, G. Zhang, and Y.-W. Zhang, Phys. Rev. B **89**, 035438 (2014).

[43] S. Neogi and D. Donadio, Eur. Phys. J. B **88**, 73 (2015).

[44] S. Neogi, J. S. Reparaz, L. F. C. Pereira, B. Graczykowski, M. Sledzinska, A. Shchepetov, M. Prunnila, J. Ahopelto, C. M. Sotomayor-Torres, and D. Donadio, ACS Nano **9**, 3820 (2015).

[45] L. F. C. Pereira and D. Donadio, Phys. Rev. B **87**, 125424 (2013).

[46] R. Peierls, Ann. Phys. **395**, 1055 (1929).

[47] M. Omini and A. Sparavigna, Phys. Rev. B **53**, 9064 (1996).

[48] W. Li, J. Carrete, N. Katcho, and N. Mingo, Comput. Phys. Commun. **185**, 1747 (2014).

[49] K. Esfarjani and H. T. Stokes, Phys. Rev. B **77**, 144112 (2008).

[50] W. Li, L. Lindsay, D. A. Broido, D. A. Stewart, and N. Mingo, Phys. Rev. B **86**, 174307 (2012).

[51] A. Sparavigna, Phys. Rev. B **66**, 174301 (2002).

[52] A. Ward, D. A. Broido, D. A. Stewart, and G. Deinzer, Phys. Rev. B **80**, 125203 (2009).

[53] S. Lee, D. Broido, K. Esfarjani, and G. Chen, Nat. Commun. **6**, 7290 (2015).

[54] A. J. Minnich, J. A. Johnson, A. J. Schmidt, K. Esfarjani, M. S. Dresselhaus, K. A. Nelson, and G. Chen, Phys. Rev. Lett. **107**, 095901 (2011).

[55] K. T. Regner, D. P. Sellan, Z. Su, C. H. Amon, A. J. H. McGaughey, and J. A. Malen, Nat. Commun. **4**, 1640 (2013).